1 Widespread stratospheric intrusion influence on summer ozone pollution over China revealed

- by multi-site ozonesondes and validated EAC4 reanalysis
- 3 Zhiheng Liao¹, Jinqiang Zhang², Meng Gao³, Zhiqiang Ma¹

- 5 1 Institute of Urban Meteorology, China Meteorological Administration, Beijing, China
- 6 2 State Key Laboratory of Atmospheric Environment and Extreme Meteorology, Institute of Atmospheric Physics,
- 7 Chinese Academy of Sciences, Beijing, China
- 8 3 Department of Geography, Hong Kong Baptist University, Hong Kong SAR, China

10 Correspondence: Z. Ma (zqma@ium.cn)

Abstract

Understanding stratospheric intrusion (SI) is crucial for elucidating atmospheric complexities and improving strategies to mitigate surface ozone (O₃) pollution. This study investigates a deep trough-induced SI event in China from June 10 to 13, 2013, based on ozonesondes from Beijing, Changchun, and Hong Kong, and validated O₃ reanalysis products. Ozonesondes from Beijing indicated notable upper-level secondary O₃ peaks (> 400 ppbv) since June 11. Tropospheric sub-high O₃ layers were observed in Changchun on June 12 (> 120 ppbv) and Hong Kong on June 13 (> 80 ppbv). Nationwide surface measurements recorded severe O₃ pollution (> 100 ppbv) from western plateaus to eastern plains over China. Together, these observations suggest a widespread influence of stratospheric O₃ intrusion. Further, the ozonesonde-validated EAC4 reanalysis reproduced the fine-scale SI structure (O₃-rich "tongue"), in turn well explaining the secondary O₃ peaks and sub-high O₃ layers in ozonesonde observations. The O₃-rich "tongue" swept through the Tibetan Plateau on June 10, triggering extreme O₃ pollution with a stratospheric contribution up to 30 ppbv (>30 %). With the trough's eastward movement, the O₃-rich "tongue" penetrated into the lower troposphere of eastern China, and then entrained into the surface layer, exacerbating surface O₃ pollution occurred in eastern China on June 13, with a stratospheric O₃ contribution of 3–15 ppbv (2–10 %). This research underscores the importance of multi-site ozonesondes in understanding stratospheric O₃ intrusions and the potential of the publicly available EAC4 reanalysis in multiyear SI analyses.

Keywords: stratospheric intrusion; secondary ozone peak; surface ozone pollution; upper-level trough; contribution

1 Introduction

Surface ozone (O_3) poses significant risks to public health and ecosystem productivity due to its strong oxidative capacity (Monks et al., 2015). While O_3 in the lower atmosphere is predominantly produced through photochemical reactions, stratospheric intrusion (SI)—the process where O_3 -rich air masses from the stratosphere descend to the lower troposphere—can also increase surface O_3 concentrations in certain regions (Akritidis et al., 2018;Skerlak et al., 2019;Dreessen, 2019). The natural SI processes complicate efforts to manage and reduce anthropogenic O_3 pollution (Zhao et al., 2025). Therefore, quantifying the SI contribution to surface O_3 is essential for developing effective air quality management strategies.

 SI is a key component of extratropical weather processes, and detecting SI events along with their influence on tropospheric chemistry has been a major scientific focus across Europe (Appenzeller and Davies, 1992;Stohl et al., 2003;Akritidis et al., 2018), North America (Hocking et al., 2007;Lin et al., 2016;Wang et al., 2020b), East Asia (Lin et al., 2021;Liu et al., 2024;Chen et al., 2024), and other extratropical regions (Zhang et al., 2024). While observational evidence confirms that SI can trigger episodic spikes in surface O₃ concentrations (Cristofanelli et al.,

2010; Langford et al., 2012; Yates et al., 2013; Lin et al., 2015; Dreessen, 2019; Ou-Yang et al., 2022; Chen et al., 2023; Chen et al., 2024), accurately quantifying this phenomenon remains difficult due to observational limitations. Traditionally, ozonesondes have served as a primary tool for SI detection, as they provide complete vertical O₃ profiles up to approximately 35 km. However, their sparse temporal and spatial coverage hinders a comprehensive understanding of how stratospheric O₃ penetrates to the surface (Chen et al., 2011; Zhao et al., 2021; Hong et al., 2024). To date, much of the current understanding of SI and its role in surface O₃ pollution has been derived from satellite observations (Li et al., 2015; Zhang et al., 2022; Jaeglé et al., 2017), atmospheric reanalysis (Chen et al., 2023; Knowland et al., 2017; Bartusek et al., 2023; Akritidis et al., 2018), and model simulations (Wang et al., 2020a;Zhao et al., 2021;Zhang et al., 2022;Chang et al., 2023;Hong et al., 2024;Luo et al., 2024;Zhao et al., 2024; Zhu et al., 2024; Skerlak et al., 2019). Yet, these approaches often lack rigorous validation against ozonesonde data, leading to substantial uncertainties in their findings. Alternatively, some studies have attempted to quantify stratospheric influences using ground-based chemical tracers, e.g., the ratio of O₃ to CO (O₃/CO) (Ma et al., 2014; Chen et al., 2024), cosmogenic sulfur-35 (35S) (Lin et al., 2016; Lin et al., 2021), and the ratio of cosmogenic beryllium-10 to beryllium-7 (10Be/1Be) (Jordan et al., 2003;Liu et al., 2024). However, these methods also exhibit limitations, as ground-based measurements alone cannot fully resolve the vertical structure of SI aloft (Zheng et al., 2024). Moreover, inconsistencies arise when different tracers are applied—for instance, while one study using ³⁵S (Lin et al., 2021) suggested a west-high-east-low SI contribution pattern over China, another study based on the O₂/CO ratio (Chen et al., 2024) reported the opposite distribution. These conflicting results reveal a significant research gap, emphasizing the necessity for comprehensive analysis of multi-platform datasets to advance our understanding of stratospheric O₃ intrusion and its effects on surface O₃ pollution.

This study examines a representative SI event triggered by an upper-level trough over China during 10-13 June 2013. The event was characterized by severe surface O_3 pollution that sequentially occurred in the high-altitude Tibetan Plateau and low-lying eastern China. To investigate the potential connection between SI processes and these O_3 pollution episodes, we employed a multi-platform integrated approach combining multi-site ozonesondes, ground-based O_3 measurements, satellite O_3 products, and atmospheric O_3 reanalysis. Through comprehensive analysis of this multi-platform datasets, we aim to address two key scientific objectives: 1) to characterize the spatiotemporal evolution of trough-induced stratospheric O_3 intrusion, 2) to quantitatively assess the SI contribution to surface O_3 pollution over different regions.

2 Datasets

2.1 Ozonesonde observation

In China, ozonesondes, along with radiosondes, were routinely launched weekly in Beijing ($116.47 \,^{\circ}$ E, $39.80 \,^{\circ}$ N) and Hong Kong ($114.17 \,^{\circ}$ E, $22.31 \,^{\circ}$ N). During June 2013, an intensive ozonesonde experiment was held in Beijing and Changchun ($125.20 \,^{\circ}$ E, $43.90 \,^{\circ}$ N), with consecutive launches from June 10-13. The details of the ozonesonde experiment can be found in Zhang et al. (2013). These sondes (including the routine ozonesonde in Hong Kong) were launched around 13:30 China Standard Time, providing high-resolution profiles of O_3 partial pressure, atmospheric pressure, temperature, and humidity from the surface up to approximately 35 km (Zhang et al., 2021;Liao et al., 2024). For this study, data from nine ozonesonde observations were analyzed to examine stratospheric O_3 intrusion during June 10-13, 2013, including four consecutive days in Beijing and Changchun, and a single launch on June 13 in Hong Kong. By comparing the sonde-based surface O_3 concentrations with ground-based O_3 measurements (Fig. 3B), we demonstrated a good accuracy of these ozonesonde observations (R = 0.981, and RAB = 3.2 ppbv).

2.2 Atmospheric reanalysis data

90 ERA5, the fifth-generation ECMWF (European Centre for Medium-Range Weather Forecasts) global reanalysis, offers a comprehensive dataset at a spatial resolution of $0.25^{\circ} \times 0.25^{\circ}$ and a temporal resolution of 1 hour for climate and weather analysis (Hersbach et al., 2020). It integrates model data with observations using four-dimensional variational assimilation in ECMWF's Integrated Forecast System (IFS). This study utilized ERA5 data, including geopotential height, potential vorticity, and wind fields, to describe the synoptic conditions during the stratospheric intrusion event.

EAC4 (ECMWF Atmospheric Composition Reanalysis 4) represents the fourth generation of ECMWF's atmospheric composition reanalysis, with a spatial resolution of $0.75 \,^{\circ} \times 0.75 \,^{\circ}$ and a temporal resolution of 3 hours (Inness et al., 2019). EAC4 assimilates data from various satellite sources, including total column O_3 from the Ozone Monitoring Instrument and Global Ozone Monitoring Experiment-2 on Metop satellites, profile data from the Microwave Limb Sounder, and partial columns from Solar Backscatter Ultra-Violet and Ozone Mapping and Profiler Suite. Note that surface O_3 measurements and ozonesonde O_3 profile data in China are not assimilated into the EAC4 reanalysis. The IFS used in EAC4 incorporates an extended version of the Carbon Bond 2005 chemical mechanism, which includes 126 tropospheric reactions. The emission datasets are composed of anthropogenic emissions from the MACCity inventory (Granier et al., 2011), biogenic emissions from MEGAN2.1 model (Guenther et al., 2006), and biomass burning emissions from the Global Fire Assimilation System (Kaiser et al., 2012). Apart from O_3 , the stratospheric O_3 tracer (O_3S , O_3 originating from the stratosphere) is also provided in EAC4 reanalysis. This study employed both O_3 and O_3S to characterize the three-dimensional structure of stratospheric O_3 intrusion.

2.3 Auxiliary data

- Additional data sources included ground-based O₃ measurements from the China National Air Quality Monitoring
 Network and the Hong Kong Environmental Protection Department, satellite cloud images from the Moderate

 Passelvtion Imagina Spectromaliameter (MODIS) satellite O₂ meadwate from the Atmospheric Infrared Soundary
- Resolution Imaging Spectroradiometer (MODIS), satellite O₃ products from the Atmospheric Infrared Sounder (AIRS) (Aumann et al., 2003), and atmospheric O₃ reanalysis from the Modern-Era Retrospective Analysis for
- (AIRS) (Aumann et al., 2003), and atmospheric O₃ reanalysis from the Modern-Era Retrospective Analysis for Research and Applications, Version 2 (MERRA2) (Gelaro et al., 2017). According to previous studies (Jaegléet al.,
- 117 Research and Applications, Version 2 (WERRA2) (Gelato et al., 2017). According to previous studies (Jaegreet al., 2017; Knowland et al., 2017; Zhang et al., 2022), we used satellite O₃ retrieved from AIRS Level 3 product, which
- has a spatial resolution of $1^{\circ} \times 1^{\circ}$. In contrast, the MERRA2 reanalysis has a spatial resolution of $0.5^{\circ} \times 0.625^{\circ}$.
- Both AIRS and MERRA2 O₃ products served as alternative references to EAC4 O₃ reanalysis to provide a
- large-scale view of horizontal and vertical O₃ structures during the SI event. Hourly surface O₃ concentrations from
- 77 cities in China (including Hong Kong) were used to assess nationwide O₃ pollution during the stratospheric
- intrusion event.

3 Results

3.1 Ozonesonde evidence of stratospheric O₃ intrusion

Fig. 1 illustrates the evolution of the upper-level trough event from June 10 to 13, 2013. On June 10, the upper-level trough extended from the Mongolian Plateau towards the Tibetan Plateau. By June 11, the trough had moved eastward and deepened into a "V-shaped" structure between 90°E and 120°E, causing an extremely distorted westerly jet and strong northerlies at the western flank of the trough. On this day, the emerged 1.5 PVU potential vorticity contours at 400 hPa provide convincing evidence for a deep stratospheric intrusion. On June 12, the "V-shaped" trough persisted at 200 hPa. By June 13, the upper-level trough had weakened to be a shallow structure over the North China Plain (NCP). Three-dimensional dynamics associated with upper-level troughs

involves stratospheric dry intrusion (SDI) and warm conveyor belts (WCB) airstreams (Browning and Roberts, 1994;Browning, 1997). The SDI originates in the lower stratosphere on the cold side of the trough (west of the trough axis) and descends behind the cold front, while the WCB originates in the warm sector of the trough (east of the trough axis), ascending rapidly to the mid- and upper troposphere. During this event, these contrasting airstreams led to significantly different weather conditions at the two sides of the trough, with cloudy weather in the WCB zone (east) and clear weather in the SDI zone (west). There appeared an obvious transition from cloudy to clear weather in the eastern China with the eastward movement of upper-level trough. On June 13, China, excluding the northeast and eastern coastal regions, experienced clear weather.

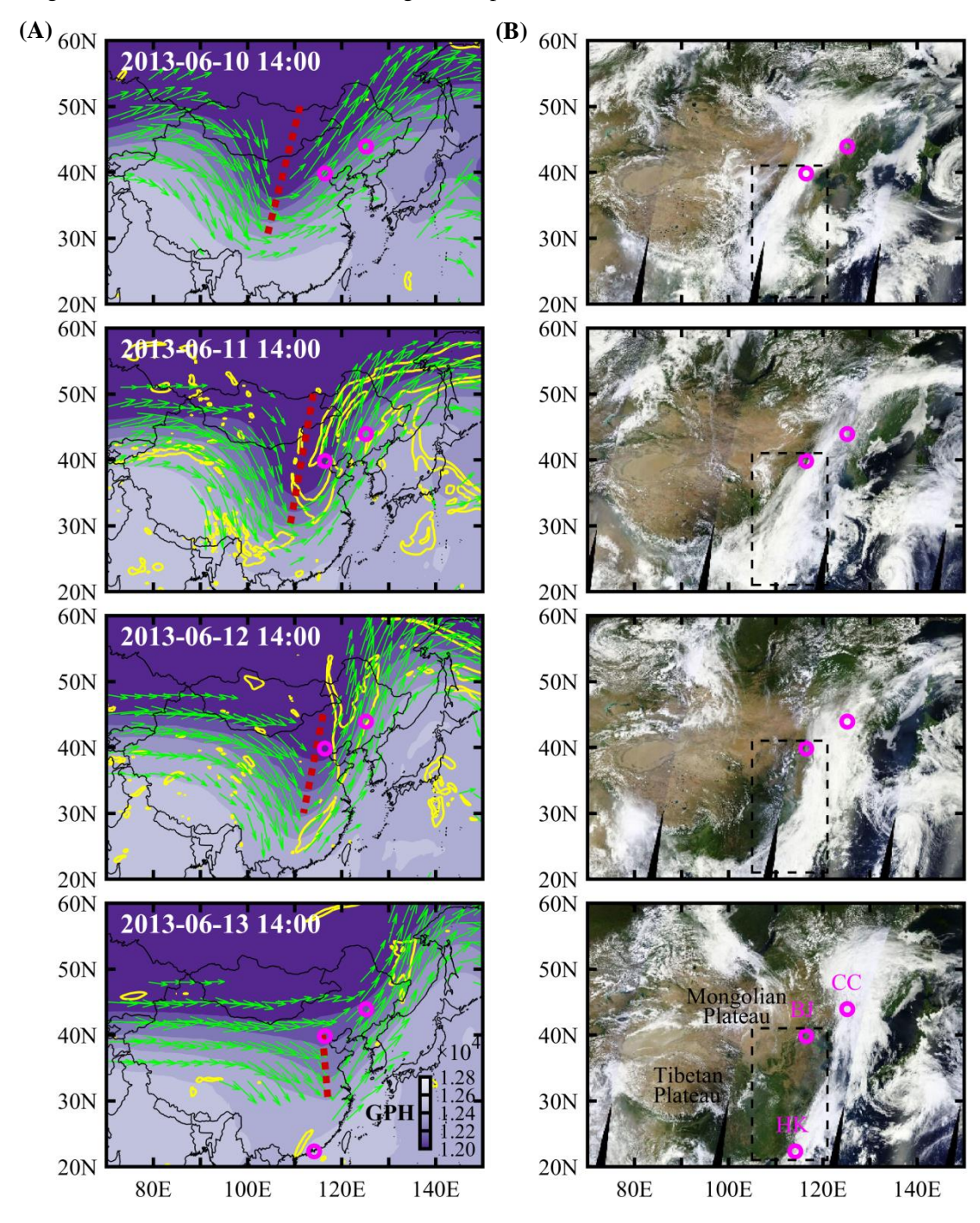


Fig. 1. (A) Horizontal distribution of geopotential height (shading, units in gpm), and wind direction of jet stream in excess of 20 m s⁻¹ (arrows) at 200 hPa, and potential vorticity of 1.5 PVU (blue contours) at 400 hPa. (B)

MODIS satellite cloud images with the dashed box marking eastern China (105 E–121 E, 21 N–41 N). Red dot lines in (A) denote the axis of upper-level trough at 200 hPa. Magenta circles mark the available ozonesondes at different sites (BJ: Beijing, CC: Changchun, and HK: Hong Kong) on different days.

146147148

149

150

151

152

153154

155

156

157 158

159

160

161

162

163

164

165

166

167

144

145

Previous ozonesonde-based observational studies (Lemoine, 2004; Hwang et al., 2007; Chen et al., 2011; Ojha et al., 2017) revealed that secondary O₃ peak in a height range between 9 and 16 km (i.e., near the tropopause) is a characteristic O₃-profile structure when SI occurs and triggers tropopause folding. The continuous and multi-site ozonesondes in this study provided a unique opportunity to characterize stratospheric O₃ intrusion linked to upper-level trough from an observational perspective (Fig. 2). On June 10, before the trough arrived, Beijing was influenced by WCB airstreams, showing high relative humidity (> 60%) in the upper troposphere. By June 11, Beijing was near the trough axis, and the O₃-rich SDI airstream began to affect the upper atmosphere, creating a secondary O₃ peak (~400 ppbv at 9.5 km height) just above the rapidly descended thermal tropopause (which dropped from 10.5 km on June 10 to 8.2 km on June 11). Besides, the cold dry air of the SDI lead to a quick drop in relative humidity from 70% on June 10 to below 25 % on June 11 in the upper troposphere of Beijing. On June 12 and 13, the secondary O₃ peaks continued to be observed over Beijing, with peak concentrations rising to 650 ppbv by June 13, but the altitude of these peaks gradually increased up to 13.6 km by June 13 with the increase of thermal tropopause height. Unlike that in Beijing, the sonde-based O₃ profiles in Changchun showed secondary O₃ peak only in June 13, when upper-level trough moved eastward to affect Changchun. However, sub-high O₃ layer (> 120 ppbv) appeared in the middle troposphere (4.2–8.1 km height, the shaded light gray in Fig. 2) in advance on June 12, accompanied by extremely low relative humidity. This sub-high O₃ layer is likely the transport result of pre-intruded O₃ from stratosphere over Beijing or its surroundings. Similar sub-high O₃ layer (> 80 ppbv) also occurred in the lower troposphere (3.5-6.0 km height, the shaded light gray in Fig. 2) of Hong Kong (a subtropical city) on June 13. These high-O₃ and low-humidity air masses in the troposphere reflect obvious stratospheric origin, suggesting a widespread SI influence from extratropics to subtropics during this deep trough event.

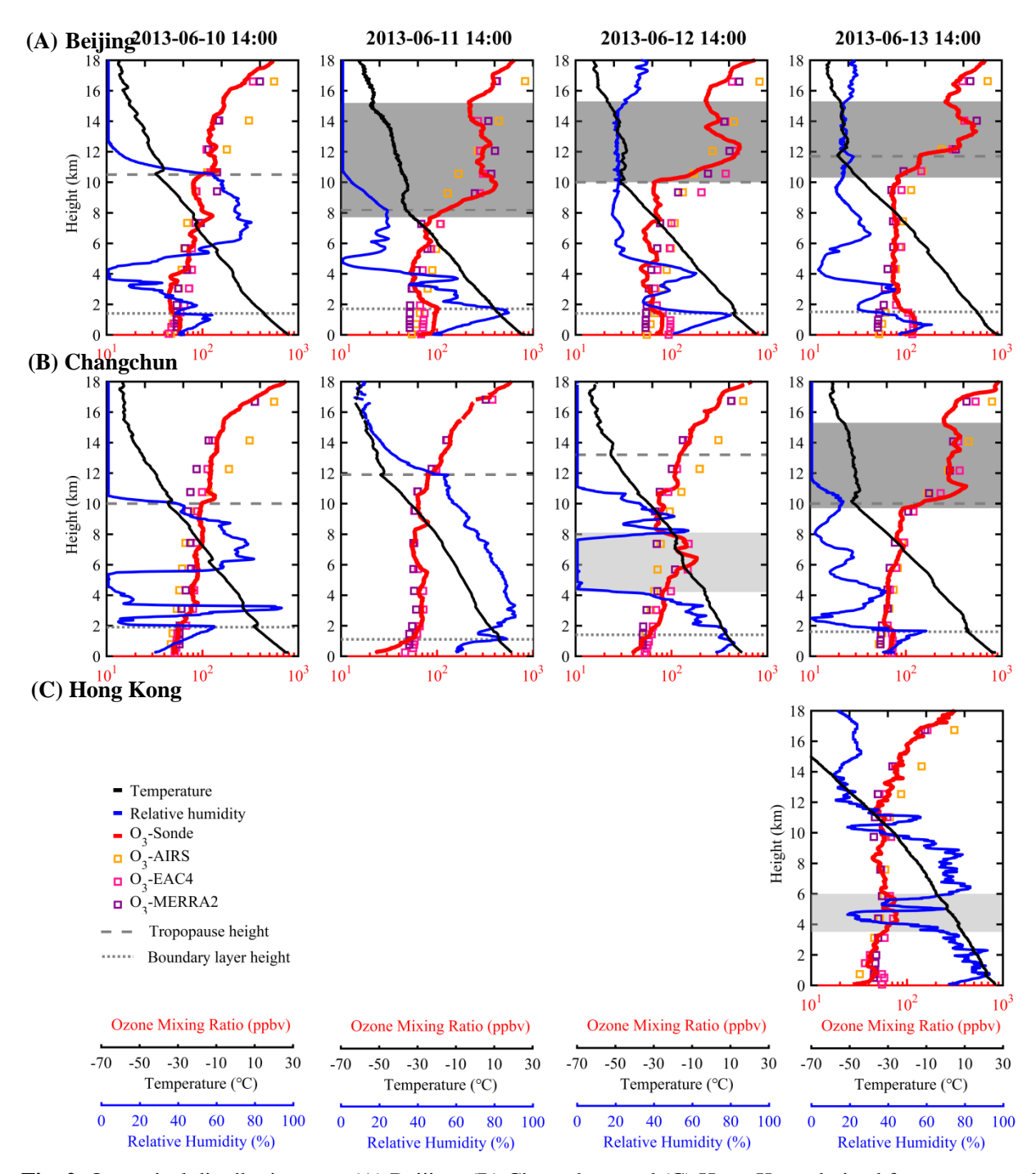


Fig. 2. O_3 vertical distribution over (A) Beijing, (B) Changchun, and (C) Hong Kong derived from ozonesonde and other data sources (including AIRS satellite observation, EAC4 and MERRA2 reanalysis) during 10–13 June 2013. Black and blue lines denote the sonde-based temperature (T) and relative humidity (RH) profiles, respectively. Gray dashed lines represent the thermal tropopause height, and gray dot lines indicate the boundary layer top height. Upper-level secondary O_3 peaks are shaded heavy gray, and SI-induced O_3 -rich layer in the troposphere is shaded light gray.

3.2 Three-dimensional structure of stratospheric O₃ intrusion

The multi-site ozonesonde observations only provide a snapshot of stratospheric O_3 intrusion. To further visualize its three-dimensional structure, we introduced the commonly-used O_3 products, including AIRS satellite

observation, MERRA2 and EAC4 reanalysis (Li et al., 2015;Knowland et al., 2017;Akritidis et al., 2018). These three large-scale O_3 products were firstly validated against our ozonesonde observations. As shown in Fig. 2, AIRS satellite observation missed the upper-level secondary O_3 peaks and the boundary-layer O_3 enhancements. MERRA2 reanalysis captured the secondary O_3 peaks but still showed large negative biases to the observed boundary-layer O_3 enhancements. In contrast, EAC4 reanalysis reproduced well the major features of the O_3 vertical distribution, including upper-level secondary O_3 peaks and boundary-layer O_3 enhancements. Particularly, EAC4 exactly captured the SI-induced sub-high O_3 layers in the middle troposphere of Changchun (on June 12) and the lower troposphere of Hong Kong (on June 13). This qualitative comparison suggests that EAC4 had a powerful ability to reproduce both the SI dynamics and boundary-layer photochemical processes. The scatter comparison with quantitative statistics in Fig. 3A further demonstrate that EAC4 O_3 reanalysis had the strongest correlation (R = 0.947), the lowest mean absolute bias (MAB = 19.1 ppbv), the lowest root mean square error (RMSE = 36.9 ppbv), and the largest index of agreement (IOA = 0.985) to the ozonesonde observation. This sonde-based validation (Fig. 3A), along with validation against with nationwide ground-based O_3 observations (Fig. 3B and Fig. 5A), provides us enough confidence in adopting EAC4 reanalysis to explore the three-dimensional structure of trough-induced stratospheric O_3 intrusion.

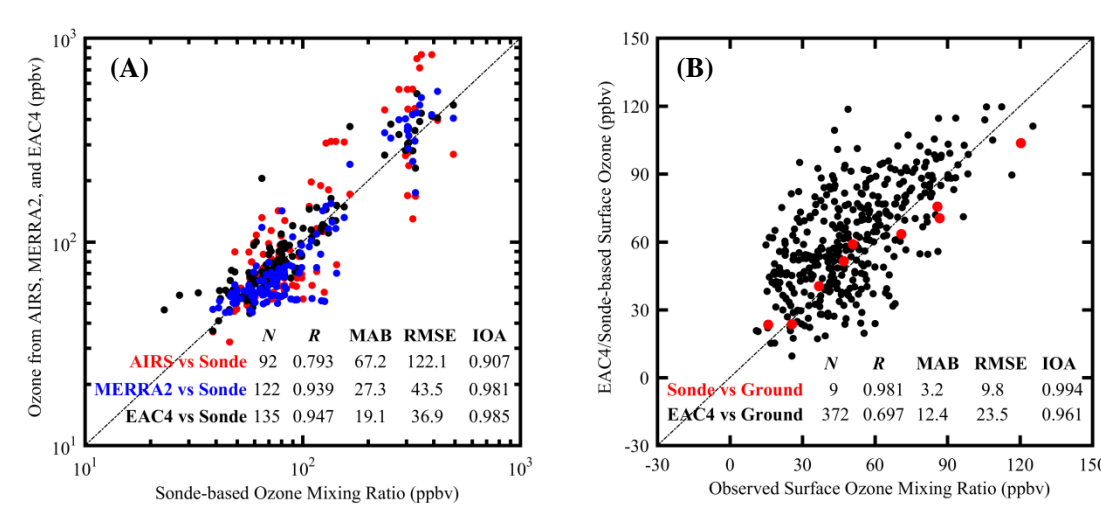


Fig. 3. (A) Validation of AIRS, MERRA2, and EAC4 O_3 products with 9 ozonesonde observations from Beijing, Changchun, and Hong Kong. (B) Validation of EAC4/Sonde-based surface O_3 concentrations with ground-based O_3 observations. In (A), AIRS, MERRA2, and EAC4 O_3 data were spatially interpolated to the location of ozonesonde stations. In (B), ground-based O_3 observations across 466 sites in 76 cities were resampled to EAC4 grid (0.75 $^{\circ}$ × 0.75 $^{\circ}$) for comparison with EAC4-based surface ozone reanalysis; ground-based O_3 observations at three neighboring sites (Tiantan site in Beijing, Daishan Park site in Changchun, and Sham Shui Po site in Hong Kong) were used for comparison with Sonde-based surface ozone concentrations. *N*, *R*, MAB, RMSE, and IOA denote the number of statistic samples, correlation coefficient, mean absolute bias, root mean square error, and index of agreement, respectively.

Fig. 4 illustrates the EAC4-based three-dimensional structure of upper-level trough-induced stratospheric O₃ intrusions over China. High O₃ concentrations at 200 hPa aligned with the trough location, extending southwestward (June 10) and southward (June 11–13) along the trough axis, which well explained the upper-level secondary O₃ peaks over Beijing since June 11 and over Changchun on June 13 (Fig. 2A and 2B). The stratospheric intrusions developed into elongated (about 2000 km) and slender (about 2000 km) streamers with elevated O₃ concentrations exceeding 150 ppbv (referred to as SDI-induced O₃-rich belts) at 400 hPa. On the east of the SDI

streamers, the WCB streamers were parallel with anomalously low O_3 concentrations (referred to as WCB-related O_3 -poor belts). On June 12, the SDI-induced O_3 -rich belt stretched to northeastern China, explaining the observed sub-high O_3 layer in the middle troposphere of Changchun (Fig. 2B). In the lower troposphere (700 hPa), O_3 -rich air masses appeared over subtropical southern China on June 11, the strongest SI day, indicating the southern edge of stratospheric O_3 intrusion. This lower-tropospheric O_3 -rich air masses persisted in subsequent days and be exactly captured by Hong Kong's ozonesonde on June 13 (Fig. 2C). From June 11 to 13, there was a significant northeastward transport and dispersion of O_3 -rich filament due to the strengthening southwesterly winds in the lower troposphere of eastern China. Through vertical and horizontal transport, lower tropospheric O_3 concentrations increased by approximately 20 ppbv across eastern China, consistent with the 18 ppbv O_3 increase observed in 2–6 km height over Beijing, indicating widespread enhancement of lower tropospheric O_3 background due to stratospheric O_3 intrusion and accumulation.

222223224

225

226

227 228

229

230 231

232

233

234235

236237

238

239

240

241

242243

244

212

213214

215

216

217

218

219

220

221

Compared with total O₃, O₃S provides a more direct view of stratospheric intrusion (Fig. 4B). The three-dimensional O₃S structure depicts the upper-level trough-induced stratospheric O₃ intrusion as a sheet-like lowering of the O₃S-rich layer along the western flank of the trough and an O₃S-rich tongue extending southward and westward from the trough base. These features aligned well with the typical structure of extratropical stratospheric intrusion associated with tropopause folding (Bithell et al., 1999; Hocking et al., 2007). On June 10, stratospheric O₃ intrusion directly hit the Tibetan Plateau, triggering extremely high surface O₃ concentrations. From June 11 to 13, the O₃S-rich tongue progressed eastward into eastern China with the trough's eastward movement. Unlike that in the Tibetan Plateau, the O₃S-rich tongue in eastern China was blocked in the lower free troposphere and did not further intrude the surface layer. This result agreed well with the observed sub-high O₃ layer in 3.5-6.0 km height over Hong Kong (Fig. 2C), suggestive of no direct stratospheric O₃ intrusion to the surface in the low-elevation eastern China. Nevertheless, these O₃-rich stratospheric air masses can be further transported into atmospheric boundary layer via convective mixing pathway, contributing to boundary layer O₃ increase. In this process, their stratospheric characteristics (high O₃, low humidity) tend to be lost due to strong turbulence mixing, eventually becoming unrecognizable in atmospheric boundary layer. Interestingly, another stratospheric intrusion induced by severe tropical storm (name: "Yagi") over the Northwest Pacific provided a parallel reference (Fig. 4B). Compared with the tropical storm-induced stratospheric O₃ instruction, the upper-level trough-induced intrusion descended to a relatively lower altitude, causing widespread O₃S signals in the atmospheric boundary layer over eastern China. Note that apart from the trough- and storm-induced SI, a secondary SI emerged in the upwind of upper-level trough on June 12 likely driven by peripheral compensatory flows. This secondary SI lead to elevated O₃ concentrations over the Mongolian Plateau (Fig. 4A). However, they were not further transported into eastern China.

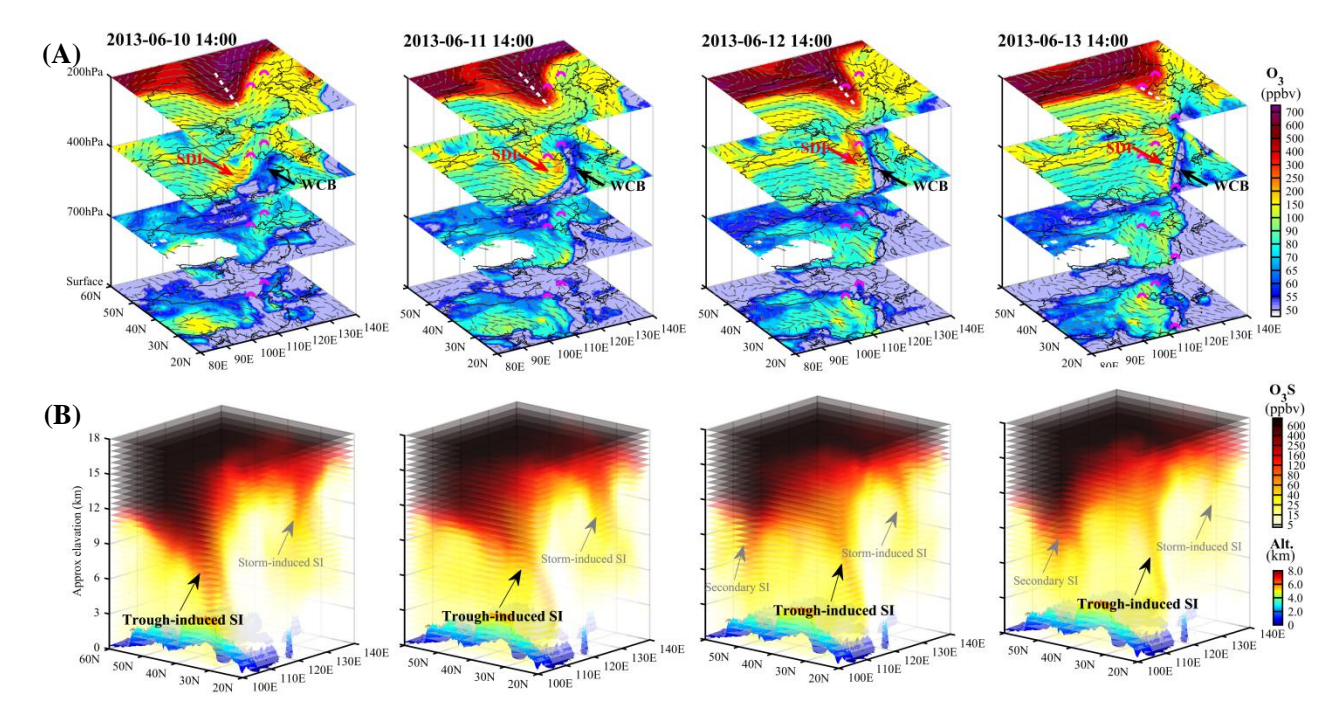


Fig. 4. (A) Spatial distribution of O_3 concentrations in 200, 400, 700 hPa, and surface layer. (B) Three-dimensional structure of O_3S concentrations. In (A), white dashed lines mark the trough axis at 200 hPa, and magenta half-circles mark the locations of ozonesondes at different sites (Beijing, Changchun and Hong Kong) on different days.

3.3 Stratospheric intrusion contribution to surface O₃ pollution

245246

247248

249

250251

252

253

254255

256257

258

259

260

261262

263

264265

266

267268

269

270

271

272

Fig. 5A presents the spatial distribution of surface O₃ concentrations derived from ground-based measurements and EAC4 reanalysis during the SI event. The EAC4-based surface O₃ reanalysis agreed well with nationwide ground-based observations (R = 0.697, MAB = 12.4 ppbv, RMSE = 23.5 ppbv, and IOA = 0.961, Fig. 3B), confirming the reliability of the EAC4 reanalysis again as the previous validation with ozonesondes. On June 10, the Tibetan Plateau experienced high O₃ concentrations near or exceeding 80 ppbv, with observed O₃ in Lhasa reaching up to 100 ppbv at 14:00 BJT. In contrast, eastern China exhibited low O₃ concentrations (< 40 ppbv) due to cloudy and rainy weather on this day. From June 10 to 13, surface O₃ concentrations decreased day by day in the Tibetan Plateau, while they increased from west to east in eastern China. By June 13, eastern China suffered severe O₃ pollution, with observed O₃ concentrations exceeding 100 ppbv in most of the NCP cities. From June 10 to 13, the continuous stratospheric dry intrusion led to a weather transition from cloudy to cloudless in eastern China (Fig. 1B), enhancing photochemical O_3 production due to the abundance of O_3 precursors over there. On the other hand, strong solar radiation in cloudless weather promoted the development of thermal convection, facilitating the mixing of pre-intruded O₃-rich stratospheric air from the lower free troposphere into the surface layer. These two mechanisms combined to trigger severe O₃ pollution in eastern China on June 13. The continue ozonesondes in Beijing provide convincing evidence for these two mechanisms. Returning to Fig. 2A, boundary-layer O₃ concentrations in Beijing increased significantly from 57.8 ppbv on June 10 to 120.6 ppbv on June 13. Considering the sharp O₃ gradient in the interface between the atmospheric boundary layer and the lower free troposphere, the dramatic increase in boundary-layer O₃ can be primarily attributed to photochemical production (Liao et al., 2024). However, the concurrent rise in O₃ concentrations in the lower free troposphere (an 18 ppbv O₃ increase in 2–6 km height from June 10 to 13) indicated that stratospheric O₃ intrusion contributed to elevating lower-tropospheric O₃ background, ultimately exacerbating boundary layer O₃ pollution.

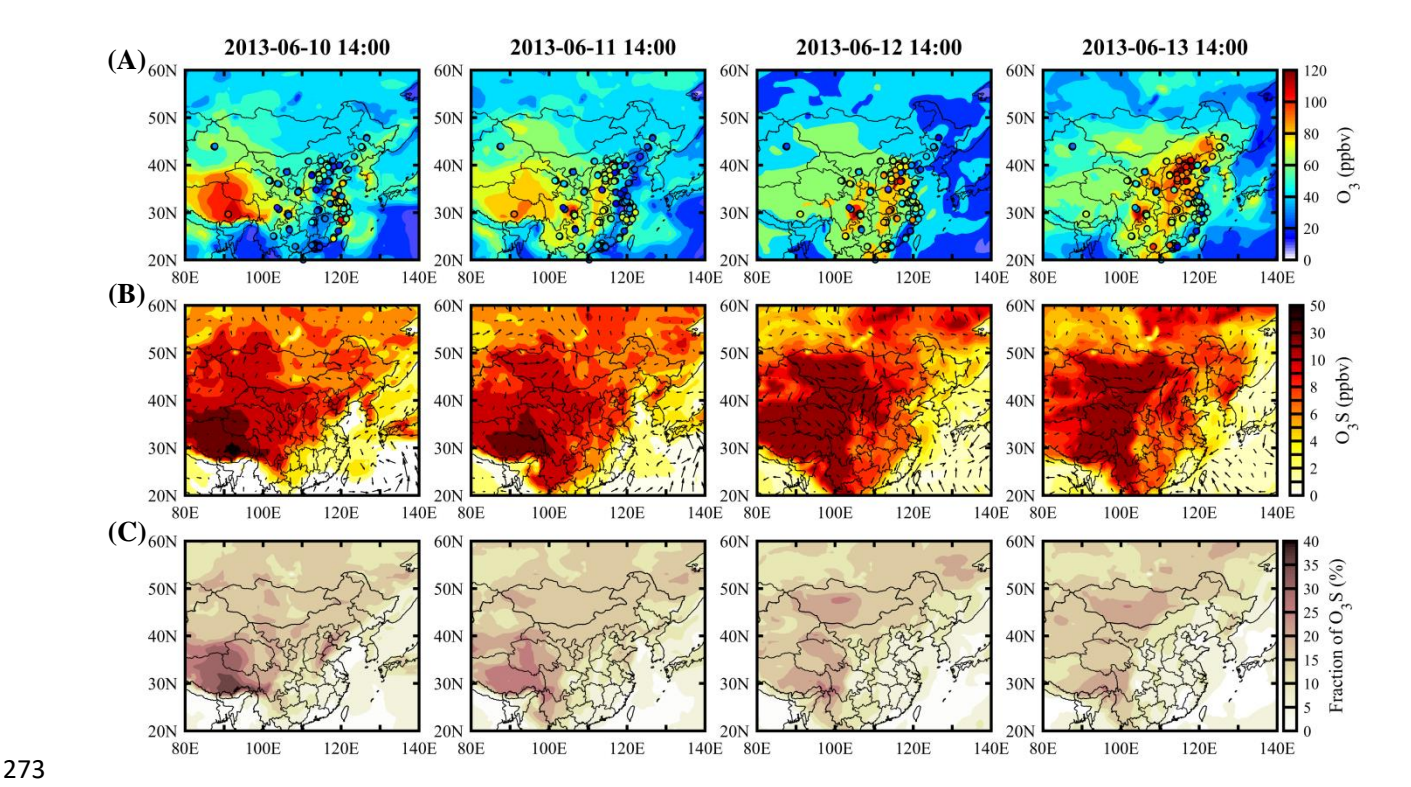


Fig. 5. (A) Surface spatial distribution of total O_3 concentration derived from ground-based measurement (dots) and EAC4 reanalysis (shading). (B) Surface spatial distribution of O_3S concentration derived from EAC4 reanalysis. (C) Spatial distribution of O_3S fraction in surface O_3 concentration calculated from EAC4 reanalysis.

To quantify the contribution of stratospheric intrusion to surface O₃ pollution, Fig. 5B illustrates the spatial distribution of EAC4-based surface O₃S concentrations during the SI event, and Fig. 5C shows the contribution fraction (CF) of O_3S in surface O_3 concentrations (CF = $100\% \times O_3S/O_3$). The high-elevation Tibetan Plateau received high-concentration O₃ from stratospheric intrusion, particularly on June 10 when the upper-level trough was oriented northeast-southwest towards the Tibetan Plateau. On this day, surface O₃S cocnentration exceeded 30 ppbv (up to 48.5 ppbv) in the Tibetan Plateau, contributing to over 30 % of the surface O₃ concentration (up to 44.7 %). Subsequent days saw a gradual decrease in O₃S over the Tibetan Plateau. On June 12 and 13, significant O₃S hotspots (> 20 ppbv) appeared in the Mongolian Plateau. In conjunction with the three-dimensional O₃S structure (Fig. 4B), the elevated O₃S concentrations in the Mongolian Plateau can be attributed to the emerged secondary SI on June 12 rather than initial trough-induced SI. It seems that the elevated O₃S in the Mongolian Plateau had no influences on surface O₃ over eastern China considering its downwind location in the lower troposphere. Nonetheless, eastern China was affected not only by the "fresh" stratospheric air in the eastward-movement O₃S-rich tongue (via convective mixing), but also by the pre-intruded "aged" stratospheric air from the Tibetan Plateau (via eastward transport). Due to continuous accumulation, region-averaged O₃S concentrations increased approximately 1.0 ppbv in eastern China from June 10 to 13, whereas their fraction in surface O₃ decreased from 11.8 % to 8.3 % as local O₃ photochemical production accelerated. On June 13, surface O₃S concentrations in eastern China ranged from 3 to 15 ppby, accounting for 2–10 % of surface O₃ concentrations. In the highly polluted NCP region, O₃S contributed approximately 10 % of surface O₃, reflecting a nonnegligible role of stratospheric O_3 intrusion in exacerbating O_3 pollution.

4 Conclusions and Discussion

274

275

276277278

279280

281

282 283

284

285

286

287 288

289 290

291

292

293

294 295

296

297

298

This study reveals that the upper-level trough-induced stratospheric O₃ intrusion over China did not occur as a local-scale vertical descent from the stratosphere to the lower troposphere just at the mid-latitude location where tropopause folding occurs; instead, it involved a long-range transport from mid-latitude tropopause folding zone (e.g., Beijing) to lower-latitude areas (e.g., Hong Kong), featuring an O₃-rich "tongue" structure with upper-level secondary O₃ peak at the base of tongue (e.g., over Beijing) and lower-tropospheric sub-high O₃ layer at the tip of tongue (e.g., over Hong Kong). The O₃-rich "tongue" swept through the high-elevation Tibetan Plateau when the upper-level trough extended towards this highland region at its initial stage, triggering extreme surface O₃ pollution. With the eastward movement of upper-level trough, the O₃-rich "tongue" penetrated into the lower troposphere of low-elevation eastern China. Over there, the intruded O₃-rich stratospheric air masses in the lower troposphere, including the "fresh" stratospheric air vertically transported from O₃-rich "tongue" and the "aged" stratospheric air horizontally transported from the Tibetan Plateau, were then entrained into the atmospheric boundary layer via lower-tropospheric dynamic processes (e.g. convective mixing). At the same time, the strengthening lower-tropospheric southwesterly winds with the eastward movement of upper-level trough gradually participated to transport these O₃-rich stratospheric air back to the mid-latitudes, ultimately exacerbating surface O₃ pollution in the NCP region (e.g., Beijing). While several SI events have been reported in China (Chang et al., 2023; Hong et al., 2024;Li et al., 2015;Luo et al., 2024;Wang et al., 2020a;Zhang et al., 2022;Zhao et al., 2024), this trough-induced SI episode may be the first event of its widespread impact and refined structure documented (Fig. 6).

315 316 317

318 319

320

321

322

323 324

325

326

327

328

329

330

331 332

333

299

300

301 302

303

304

305 306

307 308

309

310

311

312

313

314

The quantitative stratospheric intrusion contributions derived from the validated EAC4 reanalysis are generally consistent with previous model results in China. In the low-elevation eastern China, surface O₃S concentrations were previously estimated to be in the range of 5-20 ppbv during the SI events (Wang et al., 2020a; Zhang et al., 2022; Chang et al., 2023). Our EAC4-based estimation agreed well with this range, reflecting the typical magnitude of SI contribution in the low-elevation eastern China. As for the high-elevation Tibetan Plateau, a case-based model study (Skerlak et al., 2019) revealed that stratospheric tracer concentrations at the surface reach peak values of 20 % of the imposed stratospheric value, and a month-based model study (Yin et al., 2023) suggested that 36.5 % of surface O₃ in the hotspot of the southern Tibetan Plateau was contributed by stratospheric O₃ intrusion. Our EAC4-based estimation was comparable to these fractional contributions, corroborating the potential of SI to significantly influence surface O₃ concentrations in this highland region. Besides, ground-based chemical tracer method had been developed to quantify the stratospheric intrusion contribution over China. While Chen et al. (2024) identified the nationwide SI-induced O₃ enhancement as a west-low-east-high spatial distribution pattern based on surface O₃ and CO observations, Lin et al. (2021) determined a west-high-east-low spatial distribution pattern of SI-induced O₃ contribution based on ground-based cosmogenic ³⁵S observations at the Himalayas and beyond. Our result appears to support the latter, which conforms to the common knowledge that the highland regions are more susceptible to stratospheric intrusion because of their proximity to the stratosphere (Skerlak et al., 2019; Wang et al., 2020b;Lin et al., 2021).

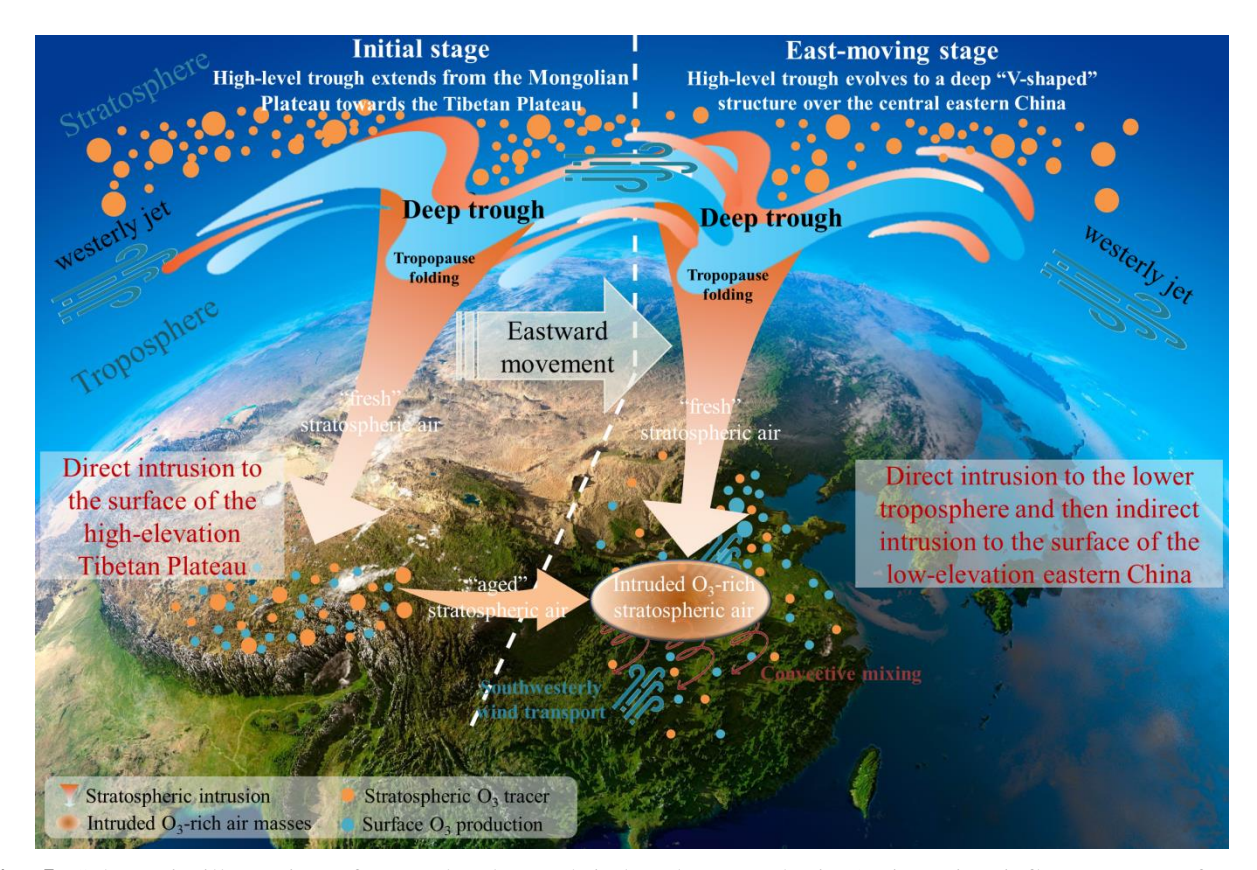


Fig. 5. Schematic illustration of upper-level trough-induced stratospheric O_3 intrusion influence on surface O_3 pollution over China

To the best of our knowledge, this study is the first to utilize continuous and multi-site ozonesondes to investigate stratospheric O₃ intrusion. While we acknowledge that a single case study may not be fully representative, it effectively demonstrates the value of continuous and multi-site ozonesonde measurements in enhancing our understanding of stratospheric O₃ intrusion phenomena. On the other hand, these continuous and multi-site ozonesondes provide a valuable and unique benchmark for examining the capacity of those commonly-used O₃ products (including AIRS satellite observation, MERRA2 and EAC4 O₃ reanalysis) in characterizing stratospheric O₃ intrusion. Previous study indicated that MERRA2 can be used in scientific studies to identify SIs by both atmospheric dynamics and composition (Knowland et al., 2017). Here, we demonstrate that EAC4, a publicly available dataset from European Centre for Medium-Range Weather Forecasts, performs better than MERRA2 in quantitatively characterizing stratospheric O₃ intrusion via comparative evaluation. Moreover, in contrast to MERRA2, EAC4 simulates full O₃ chemistry in the troposphere (an extended version of the Carbon Bond 2005 (CB05) chemical mechanism), allowing to determine the influence of stratospheric O₃ on surface concentrations separate from photochemically produced O₃. Therefore, this is a proof opening the door to detailed multiyear analyses of stratospheric O₃ intrusion and their quantitative contribution to surface O₃ over China and worldwide based on the publicly available EAC4 O₃ reanalysis.

Data availability. All used data, excluding the ozonesonde in Beijing and Changchun, are open source. ERA5 atmospheric data are available from Copernicus Climate Change Service (C3S) Climate Data Store accessible at https://cds.climate.copernicus.eu/. EAC4 O₃ reanalysis were obtained from Copernicus Atmospheric Monitoring Service Data Store accessible at https://ads.atmosphere.copernicus.eu/. The MODIS true color images are available from the NASA Earth Observations (NEO): https://neo.gsfc.nasa.gov/. The AIRS and MERRA2 O₃ products were

- 359 obtained from Goddard Earth Sciences Data and Information Services Center accessible at
- 360 https://disc.gsfc.nasa.gov/. The ozonesonde data in Hong Kong were obtained from World Ozone and Ultraviolet
- Radiation Data Centre accessible at https://woudc.org/. The ozonesonde data in Beijing and Changchun are
- available from the first author upon reasonable request (zhliao@ium.cn).

363 364

Author contributions

- 365 Z.L. conceived the original idea, analyzed the data, and wrote the first version manuscript. J.Z. designed intensive
- ozonesonde experiments in Beijing and Changchun. Z.M supervised the research project. All authors discussed the
- results and commented on the manuscript.

368 369

Competing interests

The authors declare no competing interests.

371372

370

Acknowledgements

- 373 This research has been supported by the National Natural Science Foundation of China (Grant Nos. 42405115,
- 374 42293321 and 42207115).

375

376 **References**

- Akritidis, D., Katragkou, E., Zanis, P., Pytharoulis, I., Melas, D., Flemming, J., Inness, A., Clark, H., Plu, M., and Eskes, H.: A
- deep stratosphere-to-troposphere ozone transport event over Europe simulated in CAMS global and regional forecast
- 379 systems: analysis and evaluation, Atmos Chem Phys, 18, 15515-15534, 10.5194/acp-18-15515-2018, 2018.
- 380 Appenzeller, C., and Davies, H. C.: Structure of stratospheric intrusions into the troposphere, Nature, 358, 570-572,
- 381 10.1038/358570a0, 1992.
- Aumann, H. H., Chahine, M. T., Gautier, C., Goldberg, M. D., Kalnay, E., McMillin, L. M., Revercomb, H., Rosenkranz, P. W.,
- 383 Smith, W. L., Staelin, D. H., Strow, L. L., and Susskind, J.: AIRS/AMSU/HSB on the Aqua mission: design, science objectives,
- 384 data products, and processing systems, IEEE Transactions on Geoscience and Remote Sensing, 41, 253-264,
- 385 10.1109/TGRS.2002.808356, 2003.
- Bartusek, S., Wu, Y. T., Ting, M. F., Zheng, C., Fiore, A., Sprenger, M., and Flemming, J.: Higher-Resolution Tropopause
- 387 Folding Accounts for More Stratospheric Ozone Intrusions, Geophys Res Lett, 50, ARTN e2022GL101690
- 388 10.1029/2022GL101690, 2023.
- Bithell, M., Gray, L. J., and Cox, B. D.: A Three-Dimensional View of the Evolution of Midlatitude Stratospheric Intrusions,
- 390 Journal of the Atmospheric Sciences, 56, 673-688,
- 391 https://doi.org/10.1175/1520-0469(1999)056<0673:ATDVOT>2.0.CO;2, 1999.
- 392 Browning, K. A., and Roberts, N. M.: Structure of a frontal cyclone, Q J Roy Meteor Soc, 120, 1535-1557,
- 393 https://doi.org/10.1002/qj.49712052006, 1994.
- Browning, K. A.: The dry intrusion perspective of extra-tropical cyclone development, Meteorological Applications, 4,
- 395 317-324, https://doi.org/10.1017/S1350482797000613, 1997.
- 396 Chang, F. Y., Li, J. D., Li, N., and Liao, H.: Stratospheric intrusion may aggravate widespread ozone pollution through both
- vertical and horizontal advections in eastern China during summer, Front Env Sci-Switz, 10, Artn 1115746
- 398 10.3389/Fenvs.2022.1115746, 2023.
- 399 Chen, X. L., Ma, Y. M., Kelder, H., Su, Z., and Yang, K.: On the behaviour of the tropopause folding events over the
- 400 Tibetan Plateau, Atmos Chem Phys, 11, 5113-5122, 10.5194/acp-11-5113-2011, 2011.
- 401 Chen, Z., Liu, J., Qie, X., Cheng, X., Yang, M., Shu, L., and Zang, Z.: Stratospheric influence on surface ozone pollution in
- 402 China, Nat Commun, 15, 4064, 10.1038/s41467-024-48406-x, 2024.

- 403 Chen, Z. X., Liu, J. E., Cheng, X. G., Yang, M. M., and Shu, L.: Stratospheric influences on surface ozone increase during
- 404 the COVID-19 lockdown over northern China, Npj Clim Atmos Sci, 6, Artn 76
- 405 10.1038/S41612-023-00406-2, 2023.
- 406 Cristofanelli, P., Bracci, A., Sprenger, M., Marinoni, A., Bonafè, U., Calzolari, F., Duchi, R., Laj, P., Pichon, J. M., Roccato, F.,
- 407 Venzac, H., Vuillermoz, E., and Bonasoni, P.: Tropospheric ozone variations at the Nepal Climate Observatory-Pyramid
- 408 (Himalayas, 5079 m a.s.l.) and influence of deep stratospheric intrusion events, Atmos Chem Phys, 10, 6537-6549,
- 409 10.5194/acp-10-6537-2010, 2010.
- 410 Dreessen, J.: A Sea Level Stratospheric Ozone Intrusion Event Induced within a Thunderstorm Gust Front, B Am
- 411 Meteorol Soc, 100, 1259-1275, 10.1175/Bams-D-18-0113.1, 2019.
- 412 Gelaro, R., McCarty, W., Suárez, M. J., Todling, R., Molod, A., Takacs, L., Randles, C. A., Darmenov, A., Bosilovich, M. G.,
- Reichle, R., Wargan, K., Coy, L., Cullather, R., Draper, C., Akella, S., Buchard, V., Conaty, A., da Silva, A. M., Gu, W., Kim,
- 414 G.-K., Koster, R., Lucchesi, R., Merkova, D., Nielsen, J. E., Partyka, G., Pawson, S., Putman, W., Rienecker, M., Schubert, S.
- 415 D., Sienkiewicz, M., and Zhao, B.: The Modern-Era Retrospective Analysis for Research and Applications, Version 2
- 416 (MERRA-2), Journal of Climate, 30, 5419-5454, https://doi.org/10.1175/JCLI-D-16-0758.1, 2017.
- 417 Granier, C., Bessagnet, B., Bond, T., D'Angiola, A., Denier van der Gon, H., Frost, G. J., Heil, A., Kaiser, J. W., Kinne, S.,
- 418 Klimont, Z., Kloster, S., Lamarque, J.-F., Liousse, C., Masui, T., Meleux, F., Mieville, A., Ohara, T., Raut, J.-C., Riahi, K.,
- 419 Schultz, M. G., Smith, S. J., Thompson, A., van Aardenne, J., van der Werf, G. R., and van Vuuren, D. P.: Evolution of
- 420 anthropogenic and biomass burning emissions of air pollutants at global and regional scales during the 1980–2010
- 421 period, Climatic Change, 109, 163, 10.1007/s10584-011-0154-1, 2011.
- 422 Guenther, A., Karl, T., Harley, P., Wiedinmyer, C., Palmer, P. I., and Geron, C.: Estimates of global terrestrial isoprene
- 423 emissions using MEGAN (Model of Emissions of Gases and Aerosols from Nature), Atmos. Chem. Phys., 6, 3181-3210,
- 424 10.5194/acp-6-3181-2006, 2006.
- Hersbach, H., Bell, B., Berrisford, P., Hirahara, S., Horányi, A., Muñoz-Sabater, J., Nicolas, J., Peubey, C., Radu, R.,
- Schepers, D., Simmons, A., Soci, C., Abdalla, S., Abellan, X., Balsamo, G., Bechtold, P., Biavati, G., Bidlot, J., Bonavita, M.,
- 427 De Chiara, G., Dahlgren, P., Dee, D., Diamantakis, M., Dragani, R., Flemming, J., Forbes, R., Fuentes, M., Geer, A.,
- 428 Haimberger, L., Healy, S., Hogan, R. J., Hólm, E., Janisková, M., Keeley, S., Laloyaux, P., Lopez, P., Lupu, C., Radnoti, G., de
- Rosnay, P., Rozum, I., Vamborg, F., Villaume, S., and Thépaut, J. N.: The ERA5 global reanalysis, Q J Roy Meteor Soc, 146,
- 430 1999-2049, 10.1002/gj.3803, 2020.
- 431 Hocking, W. K., Carey-Smith, T., Tarasick, D. W., Argall, P. S., Strong, K., Rochon, Y., Zawadzki, I., and Taylor, P. A.:
- 432 Detection of stratospheric ozone intrusions by windprofiler radars, Nature, 450, 281-284, 10.1038/nature06312, 2007.
- Hong, J., Wang, H., Wang, W., Zhu, J., Deng, H., and Wang, H.: Impacts of stratosphere-to-troposphere transport on
- 434 tropospheric ozone in southeastern China: insights from ozonesonde observations, Environ Res Lett, 19, 064068,
- 435 10.1088/1748-9326/ad4ef9, 2024.
- 436 Hwang, S. H., Kim, J., and Cho, G. R.: Observation of secondary ozone peaks near the tropopause over the Korean
- peninsula associated with stratosphere-troposphere exchange, J Geophys Res-Atmos, 112, Artn D16305
- 438 10.1029/2006jd007978, 2007.
- 439 Inness, A., Ades, M., Agusti-Panareda, A., Barré, J., Benedictow, A., Blechschmidt, A. M., Dominguez, J. J., Engelen, R.,
- Eskes, H., Flemming, J., Huijnen, V., Jones, L., Kipling, Z., Massart, S., Parrington, M., Pench, V. H., Razinger, M., Remy, S.,
- Schulz, M., and Suttie, M.: The CAMS reanalysis of atmospheric composition, Atmos Chem Phys, 19, 3515-3556,
- 442 10.5194/acp-19-3515-2019, 2019.
- 443 Jaeglé, L., Wood, R., and Wargan, K.: Multiyear Composite View of Ozone Enhancements and
- 444 Stratosphere-to-Troposphere Transport in Dry Intrusions of Northern Hemisphere Extratropical Cyclones, Journal of
- 445 Geophysical Research: Atmospheres, 122, 13,436-413,457, https://doi.org/10.1002/2017JD027656, 2017.
- 446 Jordan, C. E., Dibb, J. E., and Finkel, R. C.: 10Be/7Be tracer of atmospheric transport and stratosphere-troposphere

- exchange, Journal of Geophysical Research: Atmospheres, 108, https://doi.org/10.1029/2002JD002395, 2003.
- 448 Kaiser, J. W., Heil, A., Andreae, M. O., Benedetti, A., Chubarova, N., Jones, L., Morcrette, J. J., Razinger, M., Schultz, M. G.,
- Suttie, M., and van der Werf, G. R.: Biomass burning emissions estimated with a global fire assimilation system based on
- 450 observed fire radiative power, Biogeosciences, 9, 527-554, 10.5194/bg-9-527-2012, 2012.
- 451 Knowland, K. E., Ott, L. E., Duncan, B. N., and Wargan, K.: Stratospheric Intrusion-Influenced Ozone Air Quality
- 452 Exceedances Investigated in the NASA MERRA-2 Reanalysis, Geophys Res Lett, 44, 10691-10701,
- 453 10.1002/2017GL074532, 2017.
- 454 Langford, A. O., Brioude, J., Cooper, O. R., Senff, C. J., Alvarez, R. J., Hardesty, R. M., Johnson, B. J., and Oltmans, S. J.:
- 455 Stratospheric influence on surface ozone in the Los Angeles area during late spring and early summer of 2010, J
- 456 Geophys Res-Atmos, 117, Artn D00v06
- 457 10.1029/2011jd016766, 2012.
- 458 Lemoine, R.: Secondary maxima in ozone profiles, Atmos Chem Phys, 4, 1085-1096, DOI 10.5194/acp-4-1085-2004,
- 459 2004
- 460 Li, D., Bian, J. C., and Fan, Q. J.: A deep stratospheric intrusion associated with an intense cut-off low event over East
- 461 Asia, Sci China Earth Sci, 58, 116-128, 10.1007/s11430-014-4977-2, 2015.
- 462 Liao, Z., Gao, M., Zhang, J., Sun, J., Quan, J., Jia, X., Pan, Y., and Fan, S.: Mixing-layer-height-referenced ozone vertical
- 463 distribution in the lower troposphere of Chinese megacities: stratification, classification, and meteorological and
- 464 photochemical mechanisms, Atmos. Chem. Phys., 24, 3541-3557, 10.5194/acp-24-3541-2024, 2024.
- Lin, M., Su, L., Shaheen, R., Fung, J. C. H., and Thiemens, M. H.: Detection of deep stratospheric intrusions by
- 466 cosmogenic ³⁵S, P Natl Acad Sci USA, 113, 11131-11136, 10.1073/pnas.1609919113, 2016.
- Lin, M., Wang, K., Kang, S., Li, Y., Fan, Z., and Thiemens, M. H.: Isotopic signatures of stratospheric air at the Himalayas
- 468 and beyond, Sci Bull, 66, 323-326, https://doi.org/10.1016/j.scib.2020.11.005, 2021.
- Lin, M. Y., Fiore, A. M., Horowitz, L. W., Langford, A. O., Oltmans, S. J., Tarasick, D., and Rieder, H. E.: Climate variability
- 470 modulates western US ozone air quality in spring via deep stratospheric intrusions, Nat Commun, 6, Artn 7105
- 471 10.1038/Ncomms8105, 2015.
- 472 Liu, X., Fu, Y., Zhang, L., Li, H., Burr, G. S., Bi, Y., and Zhao, G.: Deep stratospheric intrusion events in China revealed on
- the ground by cosmogenic 10Be/7Be, Communications Earth & Environment, 5, 553, 10.1038/s43247-024-01727-7,
- 474 2024.
- 475 Luo, Y., Zhao, T., Meng, K., Hu, J., Yang, Q., Bai, Y., Yang, K., Fu, W., Tan, C., Zhang, Y., Zhang, Y., and Li, Z.: A mechanism of
- 476 stratospheric O3 intrusion into the atmospheric environment: a case study of the North China Plain, Atmos. Chem. Phys.,
- 477 24, 7013-7026, 10.5194/acp-24-7013-2024, 2024.
- 478 Ma, J., Lin, W. L., Zheng, X. D., Xu, X. B., Li, Z., and Yang, L. L.: Influence of air mass downward transport on the variability
- 479 of surface ozone at Xianggelila Regional Atmosphere Background Station, southwest China, Atmos Chem Phys, 14,
- 480 5311-5325, 10.5194/acp-14-5311-2014, 2014.
- 481 Monks, P. S., Archibald, A. T., Colette, A., Cooper, O., Coyle, M., Derwent, R., Fowler, D., Granier, C., Law, K. S., Mills, G. E.,
- Stevenson, D. S., Tarasova, O., Thouret, V., von Schneidemesser, E., Sommariva, R., Wild, O., and Williams, M. L.:
- 483 Tropospheric ozone and its precursors from the urban to the global scale from air quality to short-lived climate forcer,
- 484 Atmos Chem Phys, 15, 8889-8973, 10.5194/acp-15-8889-2015, 2015.
- Ojha, N., Pozzer, A., Akritidis, D., and Lelieveld, J.: Secondary ozone peaks in the troposphere over the Himalayas, Atmos
- 486 Chem Phys, 17, 6743-6757, 10.5194/acp-17-6743-2017, 2017.
- 487 Ou-Yang, C. F., Babu, S. R., Lee, J. R., Yen, M. C., Griffith, S. M., Lin, C. C., Chang, S. C., and Lin, N. H.: Detection of
- 488 stratospheric intrusion events and their role in ozone enhancement at a mountain background site in sub-tropical East
- 489 Asia, Atmos Environ, 268, ARTN 118779
- 490 10.1016/j.atmosenv.2021.118779, 2022.

- 491 Skerlak, B., Pfahl, S., Sprenger, M., and Wernli, H.: A numerical process study on the rapid transport of stratospheric air
- down to the surface over western North America and the Tibetan Plateau, Atmos Chem Phys, 19, 6535-6549,
- 493 10.5194/acp-19-6535-2019, 2019.
- 494 Stohl, A., Bonasoni, P., Cristofanelli, P., Collins, W., Feichter, J., Frank, A., Forster, C., Gerasopoulos, E., Gäggeler, H., James,
- 495 P., Kentarchos, T., Kromp-Kolb, H., Krüger, B., Land, C., Meloen, J., Papayannis, A., Priller, A., Seibert, P., Sprenger, M.,
- Roelofs, G. J., Scheel, H. E., Schnabel, C., Siegmund, P., Tobler, L., Trickl, T., Wernli, H., Wirth, V., Zanis, P., and Zerefos, C.:
- 497 Stratosphere-troposphere exchange: A review, and what we have learned from STACCATO, J Geophys Res-Atmos, 108,
- 498 Artn 8516
- 499 10.1029/2002jd002490, 2003.
- 500 Wang, H. Y., Wang, W., Huang, X., and Ding, A. J.: Impacts of stratosphere-to-troposphere-transport on summertime
- surface ozone over eastern China, Sci Bull, 65, 276-279, 10.1016/j.scib.2019.11.017, 2020a.
- 502 Wang, X. Y., Wu, Y. T., Randel, W., and Tilmes, S.: Stratospheric contribution to the summertime high surface ozone
- events over the western united states, Environ Res Lett, 15, ARTN 1040a6
- 504 10.1088/1748-9326/abba53, 2020b.
- 505 Yates, E. L., Iraci, L. T., Roby, M. C., Pierce, R. B., Johnson, M. S., Reddy, P. J., Tadic, J. M., Loewenstein, M., and Gore, W.:
- Airborne observations and modeling of springtime stratosphere-to-troposphere transport over California, Atmos Chem
- 507 Phys, 13, 12481-12494, 10.5194/acp-13-12481-2013, 2013.
- 508 Yin, X. F., Rupakheti, D., Zhang, G. S., Luo, J. L., Kang, S. C., de Foy, B., Yang, J. H., Ji, Z. M., Cong, Z. Y., Rupakheti, M., Li, P.,
- Hu, Y. L., and Zhang, Q. G.: Surface ozone over the Tibetan Plateau controlled by stratospheric intrusion, Atmos Chem
- 510 Phys, 23, 10137-10143, 10.5194/acp-23-10137-2023, 2023.
- 511 Zhang, J.-q., Xuan, Y., Xia, X.-A., Liu, M., Yan, X.-I., Pang, L., Bai, Z.-X., and Wang, X.: Performance Evaluation of a
- 512 Self-Developed Ozonesonde and Its Application in an Intensive Observational Campaign, Atmospheric and Oceanic
- 513 Science Letters, 7, 175 179, 2013.
- 514 Zhang, J., Gong, X., Crosbie, E., Diskin, G., Froyd, K., Hall, S., Kupc, A., Moore, R., Peischl, J., Rollins, A., Schwarz, J., Shook,
- M., Thompson, C., Ullmann, K., Williamson, C., Wisthaler, A., Xu, L., Ziemba, L., Brock, C. A., and Wang, J.: Stratospheric
- air intrusions promote global-scale new particle formation, Science, 385, 210-216, 10.1126/science.adn2961, 2024.
- 517 Zhang, J. Q., Li, D., Bian, J. C., Xuan, Y. J., Chen, H. B., Bai, Z. X., Wan, X. W., Zheng, X. D., Xia, X. G., and Lu, D. R.:
- 518 Long-term ozone variability in the vertical structure and integrated column over the North China Plain: results based on
- 519 ozonesonde and Dobson measurements during 2001-2019, Environ Res Lett, 16, Artn 074053
- 520 10.1088/1748-9326/Ac109f, 2021.
- 521 Zhang, Y. J., Li, J., Yang, W. Y., Du, H. Y., Tang, X., Ye, Q., Wang, Z. X., Sun, Y. L., Pan, X. L., Zhu, L. L., and Wang, Z. F.:
- 522 Influences of stratospheric intrusions to high summer surface ozone over a heavily industrialized region in northern
- 523 China, Environ Res Lett, 17, Artn 094023
- 524 10.1088/1748-9326/Ac8b24, 2022.
- Zhao, K., Chen, Y., Lian, P., Li, W., Yang, F., Zhang, X., and Yang, R.: Impact of stratospheric intrusions on surface ozone
- 526 enhancement in Hong Kong in the lower troposphere: Implications for ozone control strategy, Atmos Environ, 329,
- 527 120539, https://doi.org/10.1016/j.atmosenv.2024.120539, 2024.
- 528 Zhao, K., Chen, W., Lian, P., and Xu, D.: Optimizing Ozone Control Strategies for Chinese Megacity Clusters Under the
- 529 Influence of Stratospheric Intrusion, Journal of Geophysical Research: Atmospheres, 130, e2024JD043112,
- 530 https://doi.org/10.1029/2024JD043112, 2025.
- 531 Zhao, K. H., Huang, J. P., Wu, Y. H., Yuan, Z. B., Wang, Y. W., Li, Y., Ma, X. D., Liu, X. H., Ma, W., Wang, Y., and Zhang, X. Y.:
- Impact of Stratospheric Intrusions on Ozone Enhancement in the Lower Troposphere and Implication to Air Quality in
- Hong Kong and Other South China Regions, J Geophys Res-Atmos, 126, ARTN e2020JD033955
- 534 10.1029/2020JD033955, 2021.

the surface by a dying typhoon and shallow convection" by Chen et al. (2022), Atmos. Chem. Phys., 24, 3759-3768, 10.5194/acp-24-3759-2024, 2024.

Zhu, F., Luo, J., Wang, Z., Jin, H., Zhao, Q., Wang, Z., Luo, F., and Gu, M.: The Impact of Stratosphere-to-Troposphere Transport Associated with the Northeast China Cold Vortex on Surface Ozone Concentrations in Eastern China, Journal of Applied Meteorology and Climatology, https://doi.org/10.1175/JAMC-D-24-0027.1, 2024.

Zheng, X., Yang, W., Sun, Y., Geng, C., Liu, Y., and Xu, X.: Comment on "Transport of substantial stratospheric ozone to

535

541